

Energy gain calculations in Penning fusion systems using a bounce-averaged Fokker–Planck model

L. Chacón^{a)} and G. H. Miley

University of Illinois at Urbana-Champaign, 103 South Goodwin Avenue, Urbana, Illinois 61801

D. C. Barnes and D. A. Knoll

Los Alamos National Laboratory, Los Alamos, New Mexico 87545

(Received 31 January 2000; accepted 24 July 2000)

In spherical Penning fusion devices, a spherical cloud of electrons, confined in a Penning-like trap, creates the ion-confining electrostatic well. Fusion energy gains for these systems have been calculated in optimistic conditions (i.e., spherically uniform electrostatic well, no collisional ion-electron interactions, single ion species) using a bounce-averaged Fokker–Planck (BAFP) model. Results show that steady-state distributions in which the Maxwellian ion population is dominant correspond to lowest ion recirculation powers (and hence highest fusion energy gains). It is also shown that realistic parabolic-like wells result in better energy gains than square wells, particularly at large well depths (>100 kV). Operating regimes with fusion power to ion input power ratios (Q -value) >100 have been identified. The effect of electron losses on the Q -value has been addressed heuristically using a semianalytic model, indicating that large Q -values are still possible provided that electron particle losses are kept small and well depths are large. © 2000 American Institute of Physics. [S1070-664X(00)00711-4]

I. INTRODUCTION

The spherical inertial-electrostatic confinement (IEC) fusion concept takes advantage of the potential well generated by an inner spherical cathode (physical or virtual), biased negatively to several kV with respect to a concentric outer grounded boundary, to focus ions inward and to form a dense central core where fusion may occur. The simplest IEC device uses a physical grid to create the electrostatic well (Fig. 1). However, efficient operation of gridded IEC devices may be limited by grid overheating and erosion problems. To relieve the problem of grid erosion feared in high power scale-up units, Bussard¹ and Krall² proposed the use of a quasispherical magnetic field to replace the grid, thus creating a virtual cathode by confining electrons (Polywell™). Although grid losses are eliminated, electron power losses through the magnetic field cusps have been estimated to be deleterious.³ In order to improve the electron confinement properties, as well as the symmetry of the electron cloud, an innovative approach, based on electron confinement by a Penning-like trap to generate the virtual cathode, is being undertaken⁴ (Penning Fusion Experiment with Ions, PFX-I). The good electron confinement properties of PFX-I have been demonstrated theoretically⁵ and experimentally,^{6–8} and, recently, ion trapping in the electron well at moderate electron energies (<1 kV) has been observed experimentally.⁹

Previous theoretical analyses^{3,10} of the performance of IEC systems have concluded that these devices are unable to reach fusion breakeven due to the very large recirculation powers required to overcome the thermalizing effect of ion-ion collisions and sustain the non-Maxwellian ion profile in

velocity space. However, these studies lack a self-consistent collisional treatment of the ion distribution function in velocity space, crucial to adequately estimate the fusion rate and the recirculating power.

The present research aims to identify efficient regimes of operation of Penning IEC devices. A bounce-averaged Fokker–Planck (BAFP) model (coded as indicated in Ref. 11) has been employed for this purpose. In BAFP, only a single ion species is considered, collisional ion-electron interactions are neglected (although space charge interactions between both species are included via the Poisson equation), and electrons are assumed to form a uniform, spherically symmetric cloud.

The presentation is organized as follows. Section II describes the power balance issues of the IEC concept in detail. Section III reviews the PFX-I confinement approach. The theoretical model upon which BAFP rests is reviewed in Sec. IV. A semianalytic model has been constructed in Sec. V to provide for an independent confirmation of BAFP's numerical energy gain results, which are given in Sec. VI. Some final remarks are given in Sec. VII.

II. IEC POWER BALANCE ISSUES

The IEC concept, although potentially very attractive for reactor applications, faces several critical physics feasibility issues that may hamper its efficient operation. The different power loss mechanisms in virtual-cathode IEC devices include ion-related losses via thermalization¹⁰ and upscattering,³ as well as electron-related losses^{1,3} via radiation emission (bremsstrahlung and synchrotron radiation) or electron outflow (cusp losses, outflow from grid region). These issues are reviewed in the following sections.

^{a)}Electronic mail: chacon@lanl.gov

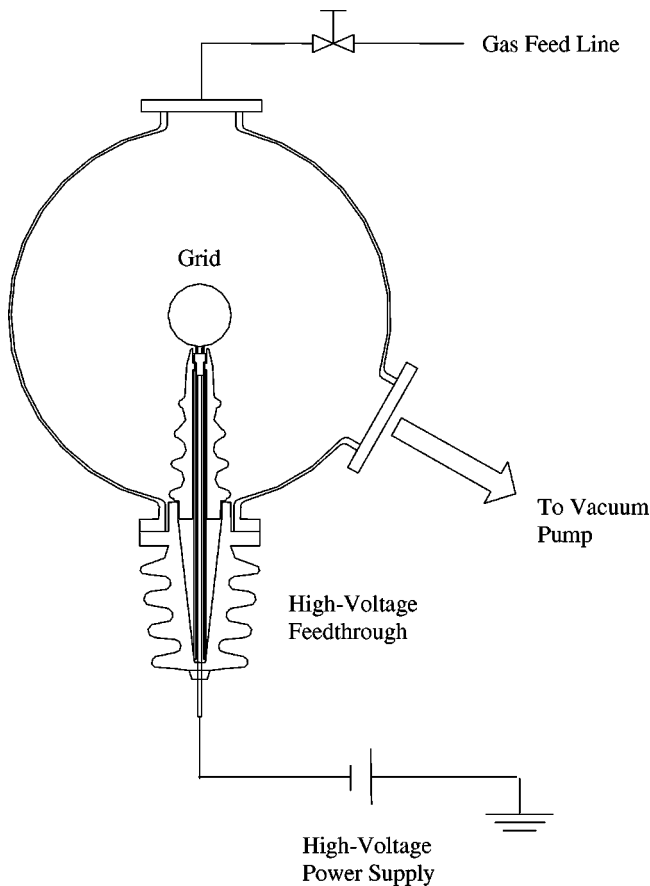


FIG. 1. Schematic of gridded IEC device (University of Illinois design).

A. Ion thermalization and upscattering

Collisional degradation of the beam-like ion distribution function is a crucial issue in the assessment of the physical feasibility of IEC devices, because it may preclude adequate ion concentration at the spherical center. Nevins¹⁰ addressed this issue by calculating collisional relaxation rates from a beam-like, monoenergetic ion population, absolutely confined in a square potential well. From his analysis, Nevins concluded that the IEC system cannot work beyond the ion-ion collisional time scale, after which the system will thermalize and lose ion focusing before enough fusion events take place. Accordingly, he predicted that the Q -value (defined as fusion power over ion input power) of IEC devices operating with a 50% deuterium–tritium (D-T) mixture would be < 0.21 for a 50 kV square well. This conclusion would rule out the possibility of a fusion reactor, but would leave open the development of driven neutron sources. Note, however, that a tightly focused monoenergetic ion beam is in fact a pessimistic scenario, because different co-moving ion species (such as D and T) with the same energy result in a finite speed difference, thus fostering ion-ion collisions and the degradation of the ion distribution function. It would be more realistic to consider that, in a square well, friction between species would homogenize the speed within the ion beam after some time, making the speed difference infinitesimal. This line of argument was pursued by Barnes *et al.*,¹² who found $Q \sim 1.3$ for the same system.

Ion upscattering losses are caused by ions picking up sufficient kinetic energy via Coulomb collisions to surmount the well and be lost from the system. According to Ref. 3, the ion upscattering time is about a thousandth of the fusion time, and thus it may represent a potential power sink.

B. Electron-related losses

Synchrotron radiation losses in IEC concepts that involve magnetic fields (PolywellTM, Penning trap, and gridded devices with magnetically protected grids) have been estimated^{1,3} to be negligible. On the other hand, bremsstrahlung radiation losses may represent an important power sink. These are minimized by utilizing low- Z fuels (D-D, D-T), and by maintaining a low electron average energy $\langle E_e \rangle$ in the system and a large ion average energy $\langle E_i \rangle$ (which in the IEC concept can be tailored via the well depth). Although this is generally not possible when both ions and electrons are in local thermodynamic equilibrium (LTE), it might be possible if the ion and electron populations are decoupled and non-Maxwellian (as is the case in the IEC high-density core¹).

In PolywellTM, electron cusp losses have been estimated³ to be prohibitive for a fusion reactor (although other authors^{1,2} claim that they can be kept at a reasonable level for efficient operation). Penning traps, on the contrary, have experimentally shown^{6–8} good electron confinement, thus virtually eliminating electron outflow power losses. In addition, Penning traps offer a simple system for analysis (because they present spherical symmetry), pending experimental confirmation of their ion focusing properties. This research focuses on this concept, which is discussed in further detail in the next section.

III. THE PENNING FUSION DEVICE

A. Principle of confinement

In the Penning Fusion device (PFX-I),^{4,8} radial electron confinement is provided by a strong axial magnetic field (≥ 0.5 T), which keeps electrons gyrating around the axial field lines. Axial electron confinement is provided by an electrostatic well of depth W_0 generated by two negatively biased end cathodes, coaxial with the magnetic field, and a grounded central anode, coaxial with the other two (Fig. 2). The central anode is onion-shaped, and is designed to induce a mirror-like perturbation in the axial magnetic field. The mirror-like magnetic field provides both radial (cyclotron orbits) and axial (mirror effect) electron confinement within the conductor, except at the polar regions (divertors), where the electrons can leak out along the axis (although they are still confined by the axial magnetic field and the end cathodes). The magnetic field is shaped so that energetic electrons cannot reach the anode wall, thus avoiding electron losses.

A high degree of sphericity of the confined electron cloud is crucial for ion focusing. This in turn requires adequate design of the anode shape and the strength of the magnetic field, and the adequate steady-state electron distribution⁸ to form a quasiuniform spherical electron cloud

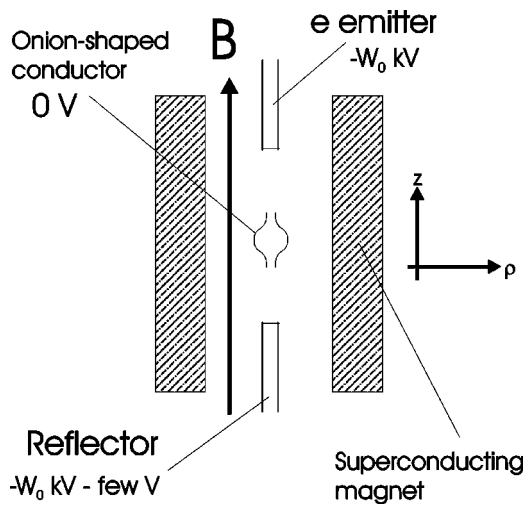


FIG. 2. Cross section of the experimental layout of the PFX-I experiment. The emitter (electron source), onion-shaped anode and reflector form an axial electrostatic well for electron axial confinement (radial confinement is provided by the axial magnetic field). The reflector is biased slightly more negative than the emitter to avoid electron losses to the reflector.

within the onion-shaped anode. The unneutralized space charge determines the maximum system size, as excessive electric field at the conductor's wall would result in surface flash-over and electrical breakdown. Practical considerations suggest that the fusion cell radius a be $< 10^{-2}$ m, with electron densities of $n_e \sim 10^{18} \text{ m}^{-3}$, and maximum electron space charge potential < 300 kV (the actual potential in the system is smaller due to space charge neutralization by ions).

Ions are electrostatically confined in PFX-I by the electron's space charge. Ions are in practical terms unmagnetized, because magnetic forces are smaller than electrostatic forces by the electron to ion mass ratio.⁸ To maintain the ion confinement, the ion inventory must be only a fraction of the electron inventory to preserve the negative space charge in the system. Hence, the Penning trap must remain a one-Debye-length machine.

It is of interest to calculate typical fusion power densities for the operation parameters specified above. For an average ion density of $\langle n_i \rangle \approx 10^{18} \text{ m}^{-3}$ confined by a 100 kV electrostatic well (which would require an electron cloud density $n_e > 2 - 3 \langle n_i \rangle$ to form) in a 10^{-2} m radius cell, and assuming a factor of 5 increase in the power density due to density peaking (see Sec. VIB), we find that the fusion power density $p_f \approx 3 \text{ kW/m}^3$ for a 50% D-T mixture. Increasing the fusion power density further requires increasing the electron density n_e and decreasing the fusion cell radius a , while maintaining the well depth ≈ 100 kV (to maximize the fusion reactivity). For a fixed well depth of 100 kV, the electrostatic Poisson equation yields $n_e \propto a^{-2}$, and since $n_e \propto \langle n_i \rangle$, we find $p_f \approx 3(0.01/a)^4 \text{ kW/m}^3$, and the total fusion power per cell $P_f \approx 1.25 \cdot 10^{-4}/a(\text{m}) \text{ W}$ (note that, for a fixed well depth, P_f increases as the cell radius a decreases). Thus, if the fusion cell radius is reduced to $a \approx 4 \cdot 10^{-3}$ m, the fusion power density increases to $p_f \approx 0.12 \text{ MW/m}^3$ and the total

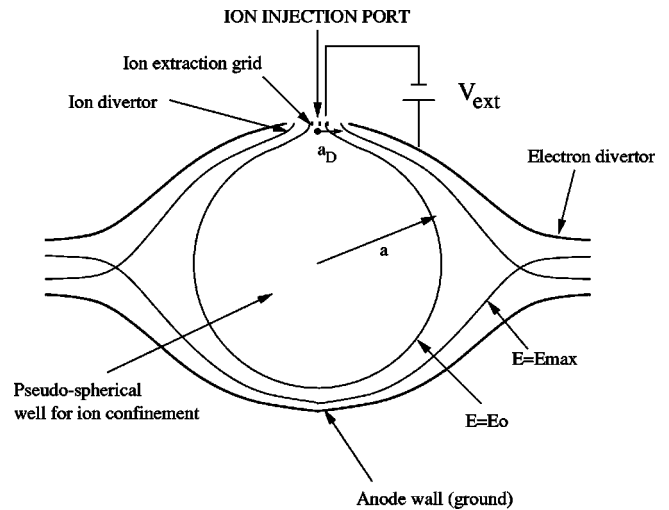


FIG. 3. Detail of the anode and the ion injection port in PFX-I (not to scale). Ion and electron divertors are indicated, as well as the E_0 and E_{max} equipotential lines that define the ion confinement region. The E_0 contour line determines the region of absolute ion confinement.

fusion power per cell is $P_f \approx 0.03 \text{ W}$. Admittedly, due to the small volume per cell, a large number of Penning fusion cells would be required for a decent-sized fusion reactor (about $3 \cdot 10^7$ cells would be required for a 1 MW reactor), and the question remains about the engineering challenges of such a system (refer to Refs. 13 and 14 for proposed fusion reactor concepts based on Penning fusion cells).

Ions may be introduced in the system in two ways: by injection or by electron impact ionization (EII) of a neutral gas. In the latter case, the system would rely on EII of a very low density, low pressure fusionable neutral gas to generate an ion cloud, which would be confined by the electron space charge. The disadvantage of this is that there is little control over the ion source shape in energy space, essential in steady-state operation. However, EII is a valid scheme in pulsed operation, as has been recently proposed^{14,15} in the periodically oscillating plasma sphere (POPS) concept.

Ion injection, however, allows controlling the shape of the ion source in energy space, and is the one considered in the steady-state analysis performed in this work. Ions can be injected in the system through a lateral injection hole on the anode wall (Fig. 3). In addition to the magnetic insulation of the anode provided by the magnetic field, the ion extraction grid should be negatively biased with respect to the anode wall, to prevent electron leakage through the ion injection port [which would present a large power sink, because electrons have the largest kinetic energy ($\sim W_0$) within the anode] and also prevent ion leakage through the electron divertors (which would also present a large power sink, because ions would accelerate to the whole electron well depth W_0 before being collected). The effectiveness of the ion extraction grid bias in preventing ion and electron losses depends substantially on the actual trap design, and is uncertain at this point. It will be assumed in what follows that no particle losses occur via this mechanism.

B. Time scales in PFX-I

Four different time scales pertain to ions in this system:

- (1) The *ion bounce time* τ_b : time that an ion takes to complete a closed orbit in the spherical well. It can be estimated by $\tau_b \sim 4a/v_b$, where a is the radius of the pseudospherical ion well (Fig. 3) within the anode, and $v_b = \sqrt{2E_0/m}$, with E_0 the ion well depth (potential difference between the bottom of the well and the ion injection grid, which is the last closed equipotential line; see Fig. 3), and m the ion mass. In a typical system, $a \sim 10^{-2}$ m, and $E_0 \sim 100$ kV, and hence $\tau_b \sim 10^{-8}$ s.
- (2) The *ion replacement time* τ_i : time that an ion injected with total energy (kinetic plus potential) equal to the energy of the potential well boundary E_{\max} (which is chosen as the equipotential line that corresponds to the X-point in the electron divertor; see Fig. 3) takes to get out of the system in the absence of collision events. Since the ion total energy is equal to the well depth, the ion will recirculate in the trap until it finds the ion divertor (Fig. 3), through which the ion will exit. Hence, the ion replacement time is given by $\tau_i = \tau_b/f_D$, where f_D represents the probability that ions find the ion divertor (Fig. 3) while recirculating. This probability can be estimated, assuming the angular motion of ions is ergodic in the well, as the ratio of the injection port area to the cell boundary area, $f_D \approx \pi a_D^2/4\pi a^2 = (a_D/2a)^2$, where a_D is the ion divertor radius (Fig. 3). Typically, $f_D \sim 10^{-6} - 10^{-4}$, and hence $\tau_i \sim 10^{-4} - 10^{-2}$ s.
- (3) The *ion-ion collision time* τ_{ii} : it can be estimated using¹⁶

$$\tau_{ii} \sim \frac{\sqrt{m}E_0^{3/2}}{\sqrt{2}\pi(k_0e^2)^2\langle n_i \rangle \Lambda}, \quad (1)$$

where $\langle n_i \rangle$ is the ion average density, E_0 is the well depth in the *absence* of ions, Λ is the Coulomb logarithm (assumed equal to 20 throughout this document), $k_0 = 1/4\pi\epsilon_0$ is the permittivity constant, and e, m are the ion charge and mass, respectively. For typical parameters in the Penning fusion cell ($\langle n_i \rangle \sim 10^{18}$ m⁻³ and $E_0 \sim 100$ kV), $\tau_{ii} \sim 0.1$ s.

- (4) The *ion-electron collision time* τ_{ie} : estimated as the reciprocal of the collision frequency of a fast electron beam (~ 100 keV) impinging on a target Maxwellian ion population, $\nu_{\epsilon}^{e/i}$.¹⁶ In units of the ion-ion collision frequency $\nu_{ii} = \tau_{ii}^{-1}$, there results

$$\frac{\nu_{\epsilon}^{e/i}}{\nu_{ii}} \sim 0.1 \left(\frac{T}{E} \right) \left\{ \sqrt{\frac{T}{E\mu}} - 8.9 \cdot 10^4 \mu \exp \left[-\frac{1836\mu E}{T} \right] \right\},$$

where μ is the ion mass in proton mass units ($\mu \sim 2.5$ for a 50% D-T mixture), E is electron energy, and T is the ion temperature (ions are assumed to be Maxwellian). Typically, $T/E \sim 0.1$, and $\tau_{ie} = [\nu_{\epsilon}^{e/i}]^{-1} \sim 10 - 100$ s.

Thus, for typical operating conditions, the time scale hierarchy in PFX-I is

$$\tau_b \sim 10^{-8} \text{ s}; \quad \tau_i \sim 10^{-4} - 10^{-2} \text{ s}; \quad \tau_{ii} \sim 0.1 \text{ s}; \quad \tau_{ie} \sim 10 - 100 \text{ s}.$$

IV. THE BAFP MODEL

In principle, to model the system accurately, the general form of the Boltzmann transport equation would have to be solved for all the species in the system, namely, multiple ion species and electrons. However, such a problem is extremely difficult to solve, due to the disparity of time scales present and the number of nonlinear equations to be solved simultaneously.

Fortunately, the problem can be substantially simplified on the grounds of the time scale analysis performed in the previous section. Thus, $\tau_{ie} \gg \tau_{ii}$ suggests that the ion and electron physics are decoupled in the ion-ion collision time scale. Accordingly, ion-electron collisional interactions can be neglected, and the problem can be modeled by considering the Fokker–Planck transport equation of the ion species alone. The problem will be simplified further by treating a 50% D-T mixture as a single ion species of mass $m = (m_D + m_T)/2$.

Spatial spherical symmetry is assumed, thus neglecting boundary effects of injection ports. The ion transport governing equations can then be expressed as¹¹

$$\frac{\partial f}{\partial t} + v_r \frac{\partial f}{\partial r} - \frac{e}{m} \frac{d\Phi}{dr} \frac{\partial f}{\partial v_r} = L(f), \quad (2)$$

$$\frac{1}{r^2} \frac{d}{dr} \left(r^2 \frac{d\Phi}{dr} \right) = \frac{e}{\epsilon_0} \left[n_e - \int d\mathbf{v} f(r, \mathbf{v}, t) \right], \quad (3)$$

where $f(r, v_r, v_p)$ is the ion distribution function in phase space, $\Phi(r)$ is the electrostatic potential within the trap, n_e is the electron density (which is taken here as uniform), and $L(f)$ is the Fokker–Planck collision operator, which in the Rosenbluth form¹⁷ reads

$$L(f) = -\frac{4\pi(k_0e^2)^2\Lambda}{m^2} \times \frac{\partial}{\partial \mathbf{v}} \cdot \left[f \frac{\partial H(f)}{\partial \mathbf{v}} - \frac{1}{2} \frac{\partial}{\partial \mathbf{v}} \cdot \left(\frac{\partial^2 G(f)}{\partial \mathbf{v} \partial \mathbf{v}} f \right) \right]. \quad (4)$$

The coefficients in $L(f)$ are expressed in terms of the Rosenbluth potentials $H(f)$ and $G(f)$, defined as $\nabla_{\mathbf{v}}^2 H = -8\pi f$ and $\nabla_{\mathbf{v}}^2 G = H$, respectively.¹⁷

Since $\tau_b \ll \tau_{ii}$, and interesting physics occur in the τ_{ii} time scale, τ_b should be removed from the theoretical formulation because it is a source of numerical stiffness. This is done by averaging the Fokker–Planck transport equation along one closed particle orbit (bounce average). As a result, the bounce-averaged Fokker–Planck transport equation reads¹¹

$$\frac{\partial g}{\partial t}(E', L, t) = \oint_{E', L} d\tau_b L(f) + S(E', L) - \nu_i(E') g(E', L, t), \quad (5)$$

where $g(E', L, t) = \tau_b(E', L, \Phi) F(E', L, t)$, with $\tau_b(E', L, \Phi)$ the bounce time (which is strongly dependent on the potential profile Φ), and $F(E', L, t)$ the ion distribution in Vlasov space, which is a function of the angular momentum, L , and the *effective* radial ion energy at $r = a$, $E' = E - L^2/2ma^2$ (where E is the total ion energy). These are all constants of motion in the ion bounce time scale.

In Eq. (5), $S(E', L)$ is the ion source, and $\nu_i(E')$ is the ion loss frequency. Ion sources and sinks can be naturally characterized in terms of the effective ion radial energy E' ,¹¹ because ions enter and exit the system at the outer cell radius (ion sources and sinks are imposed as boundary conditions at $r=a$ in the full theoretical formulation). There are two possible mechanisms for ions to be lost from the fusion cell: either they escape through the ion divertor (with center-point potential energy E_0), or they escape the well boundary (of potential E_{\max} see Fig. 3) and are lost in a single bounce. As ions with radial energies below E_0 are absolutely confined in the trap in the absence of collision events, E_0 is taken as the reference for the ion potential well. According to these different ion loss paths, three different confinement regions can be identified according to the value of E' :

- (1) *Ion confinement region*: $E' \leq E_0$. Ions are absolutely confined in this region, and hence $\nu_i(E') = 0$.
- (2) *Fast ion loss region*: $E_{\max} < E' < E_{\text{dom}}$, where E_{dom} is the numerical domain limit. The ion loss frequency is characterized by the ion bounce time, τ_b , and hence $\nu_i(E') = \tau_b^{-1}$.
- (3) *Slow ion loss region*: $E_0 < E' < E_{\max}$. In this region, $\nu_i(E')$ is characterized by the ion replacement time, τ_i , and its form is intimately related to the potential profile in the ion divertor. For a simple vacuum model of this potential profile, the ion loss frequency for $E' \in (E_0, E_{\max})$ can be expressed as¹¹

$$\nu_i(E') = \frac{1}{\tau_i} \frac{E' - E_0}{E_{\max} - E_0}. \quad (6)$$

The ion source $S(E', L)$ in Vlasov space has to be located in the ion loss region, as an ion injected in the system will have a minimum energy (relative to the bottom of the well) of $E = E_0$. A Gaussian profile is selected for the ion source in the ion loss region, centered at (E_s, L_s) , and with deviations σ_{E_s} and σ_{L_s} ,

$$S(E', L) = \begin{cases} S_{\max} \exp\left(-\frac{(E' - E_s)^2}{2\sigma_{E_s}^2} - \frac{(L - L_s)^2}{2\sigma_{L_s}^2}\right), & E' > E_0 \\ 0, & E' < E_0 \end{cases}. \quad (7)$$

Here, E_s is the ion injection energy, which satisfies $E_0 < E_s < E_{\max}$. The first inequality stems from the constraint indicated above; the second inequality is imposed for efficiency, since ions with $E > E_{\max}$ will be lost in one bounce. Also from efficiency considerations, $2\sigma_{E_s} \ll E_{\max} - E_0$, so that the majority of the ion source distribution is effectively contained in the slow ion loss region. The rest of the source parameters $S_{\max}, L_s, \sigma_{L_s}$ are arbitrary; in computations herein, we take $\sigma_{L_s} = \sigma_{E_s} = \sigma_s$, and $L_s = 0$.

A. Properties of the steady-state solution

A steady state occurs when $\partial g / \partial t = 0$. According to Eq. (5), the steady-state solution satisfies

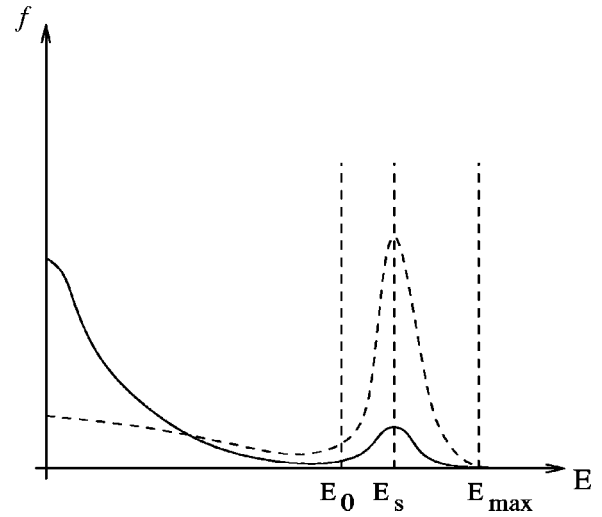


FIG. 4. Sketch of two opposite limits of the beam-Maxwellian equilibrium: the solid line corresponds to a case in which the Maxwellian population is dominant; the dashed line corresponds to a case in which the beam contribution is dominant.

$$\nu_i(E') g(E', L) = \oint_{E', L} d\tau_b L(f) + S(E', L); \quad E' > E_0 \quad (8)$$

$$\oint_{E', L} d\tau_b L(f) = 0; \quad E' < E_0. \quad (9)$$

Condition (9) is satisfied by the Maxwellian distribution f_{MB} , since $L(f_{MB}) = 0$. Hence, the steady-state distribution function in the trap will be formed by a beam-like component in the ion loss region ($E' > E_0$), determined by the ion source and sink strengths, and a Maxwellian component in the ion confinement region ($E' < E_0$), with temperature and particle number determined by collisional equilibrium with the beam. Two opposite limits of this kind of solution are depicted in Fig. 4. The realization of either of these limits depends on the equilibrium between two competing effects, namely, upscattering of the Maxwellian ion population confined in the well (which increases as the Maxwellian temperature increases, and tends to empty the well), and downscattering of the beam (which tends to fill it). The relative importance of these effects is directly related to the strength of the source and the sink in the problem, which are characterized here by S_{\max} (maximum value of the ion source) and τ_i (ion replacement time), respectively. Thus, weak sinks and strong sources will result in a large beam population, thus increasing the beam downscattering rate and hence increasing the Maxwellian temperature, resulting in the dotted line profile in Fig. 4. Conversely, weak sources and strong sinks will result in a small beam population, thus decreasing the beam downscattering rate and resulting in smaller Maxwellian temperatures, leading to the solid line profile in Fig. 4.

In steady state, particle sources and sinks in the ion loss region ($E' > E_0$) have to be in equilibrium. Thus, taking the particle and energy moments of Eq. (8) in Vlasov space, and noting that the particle and energy moments in Vlasov space of $\oint_{E', L} d\tau_b L(f)$ cancel,¹¹ yields

$$\int dE' dL^2 S(E', L) = \int dE' dL^2 v_i(E') g(E', L), \quad (10)$$

$$\int dE' dL^2 E S(E', L) = \int dE' dL^2 E v_i(E') g(E', L), \quad (11)$$

where $E' = E - (L^2/2ma^2)$, and $dL^2 = 2LdL$.

B. Calculation of energy gains

Input powers to the system are the electron injection power $P_{e,\text{in}}$ (to sustain the well) and the ion injection power P_{in} (to maintain a steady-state ion distribution). Output powers include the ion upscattering power loss P_{loss} , the electron upscattering power loss $P_{e,\text{loss}}$, the radiative power loss P_{Br} , and fusion power P_f . In steady state, $P_{e,\text{loss}} + P_{\text{Br}} + P_{\text{loss}} = P_{\text{in}} + P_{e,\text{in}}$. Clearly, for efficient operation, it is of interest that

$$P_f \gg P_{\text{in}} + P_{e,\text{in}} = P_{\text{loss}} + P_{e,\text{loss}} + P_{\text{Br}}. \quad (12)$$

Hence, the proof-of-principle energy gain definition reads

$$Q_{\text{pop}} = \frac{P_f}{P_{\text{loss}} + P_{e,\text{loss}} + P_{\text{Br}}}. \quad (13)$$

An accurate calculation of all these power losses requires modeling both ions and electrons self-consistently. At present, however, the model treats only ions self-consistently, and only ion losses (P_{loss}) are calculated. This research will concentrate on the task of showing which regimes of operation in spherical, Penning IEC devices satisfy $Q = P_f/P_{\text{loss}} \gg 1$ (necessary condition for $Q_{\text{pop}} \gg 1$). How different Q and Q_{pop} are depends on the magnitude of electron power losses. Even though a *self-consistent* treatment of electrons in the system is postponed (awaiting positive conclusions from the ion energy gain analysis), some of the effects of electron losses on the gain will be *heuristically* addressed in Sec. VI C.

The fusion power P_f in the system is calculated as

$$P_f = \frac{4\pi}{3} K_{\text{fuel}} Y_{\text{fuel}} \int d(r^3) d\mathbf{v} d\mathbf{v}' f(r, \mathbf{v}) f(r, \mathbf{v}') \sigma_f(E_{\text{rel}}) v_{\text{rel}}, \quad (14)$$

where, for a particular fusion fuel,

- (1) Y_{fuel} is the energy yield per fusion event.
- (2) K_{fuel} is a constant that takes into account either density proportions in fuel mixtures, or identical-particle contributions in single-isotope fuels.
- (3) $v_{\text{rel}} = |\mathbf{v} - \mathbf{v}'|$ is the relative particle velocity.
- (4) σ_f is the fusion cross section. Here, the Bosch and Hale fusion cross section fit¹⁸ is used. This fit is in terms of the energy in the center-of-mass reference system, $E_{\text{rel}} = m_r v_{\text{rel}}^2/2$, where m_r is the reduced mass.

This work assumes a 50% D-T fuel mixture; hence, $Y_{\text{fuel}} = 17.6 \text{ MeV}$, $K_{\text{fuel}} = 1/4$, and $m_r = m_D m_T / (m_D + m_T) = 6/5$. The integral has been successfully benchmarked against the Maxwellian $\langle \sigma v \rangle$ solutions for D-D and D-T fuels (as given in Ref. 18), with accuracy in the energy range of interest (50–200 keV) on the order of a percent.

The ion loss power P_{loss} over the top of the well is given by

$$P_{\text{loss}} = \frac{8\pi^2}{m^3} \int dE' dL^2 (E - E_0) v_i(E') g(E', L).$$

Alternatively, in the absence of electron losses and once a steady state is reached in the system, P_{loss} can be obtained by calculating the *steady-state* input power P_{in} , as follows:

$$P_{\text{in}} = \frac{8\pi^2}{m^3} \int dE' dL^2 (E - E_0) S(E', L),$$

since, according to Eqs. (10) and (11), $P_{\text{in}} = P_{\text{loss}}$ in steady state. Then, the energy gain reads

$$Q = \frac{\frac{4\pi}{3} K_{\text{fuel}} Y_{\text{fuel}} \int d(r^3) d\mathbf{v} d\mathbf{v}' f(r, \mathbf{v}) f(r, \mathbf{v}') \sigma_f(E_{\text{rel}}) v_{\text{rel}}}{\frac{8\pi^2}{m^3} \int dE dL^2 (E - E_0) S(E', L)}.$$

At this point, we define the volume-averaged reactivity $\langle \sigma v \rangle_{\text{vol}}$ and the normalized input power \hat{P}_{in} as

$$\int d(r^3) d\mathbf{v} d\mathbf{v}' f(r, \mathbf{v}) f(r, \mathbf{v}') \sigma_f(E_{\text{rel}}) v_{\text{rel}} = a^3 \langle n_i \rangle^2 \langle \sigma v \rangle_{\text{vol}},$$

$$\frac{8\pi^2}{m^3} \int dE dL^2 (E - E_0) S(E', L) = \frac{E_0 a^3 \langle n_i \rangle}{\tau_{ii}} \hat{P}_{\text{in}}.$$

Using Eq. (1), the Q -value reads

$$Q = \frac{2^{3/2} K_{\text{fuel}} Y_{\text{fuel}} \sqrt{m E_0} \langle \sigma v \rangle_{\text{vol}}}{3 (k_0 e^2)^2 \Lambda \hat{P}_{\text{in}}}. \quad (15)$$

From the definition of \hat{P}_{in} , it is clearly of interest to inject ions with minimum energy above the well ($E \rightarrow E_0$) in order to obtain large gains from the system. However, there are limits to this, because the ion source distribution will always present some spread [embodied in the deviations σ_{E_S} and σ_{L_S} in Eq. (7)]. In this work, it is assumed that the ion injection kinetic energy over the top of the well is 4%–14% of the ion well depth.

C. Limitations of the BAFP model

This model assumes perfect spherical symmetry in the system, and includes ion-ion Coulomb interactions and self-consistent space charge effects. No electron collisional information is included, and only a single ion species is considered. This theoretical framework has been specifically tailored to address the ion physics self-consistently in the ion-ion collision time scale, to explore the fusion energy multiplication limits of these devices, and calculate their envelope of performance. Thus, the model will not be able to address the effects in the energy gain of ion-electron interactions or asymmetries in the confinement. These issues, although crucial in a proof-of-principle-type scenario, are secondary at this stage of the research, and should be considered only if conclusions from this analysis are positive.

V. SEMIANALYTIC BENCHMARKING MODEL

This section is devoted to the development of a semianalytic model that captures the essence of the physics in the problem, to provide independent confirmation of the results obtained from the bounce-averaged model.

As discussed in Sec. IV A, the steady-state solution to the bounce-averaged Fokker–Planck equation is formed by a beam-like component in the ion loss region ($E' > E_0$), and a Maxwellian component in the ion confinement region ($E' < E_0$), with temperature and particle number determined by collisional equilibrium with the beam. The semianalytic model treats both particle populations as separate entities that remain in equilibrium. Particles are assumed to be confined by a one-dimensional square well in Cartesian geometry, of depth E_0 . Thus, there is no spherical convergence, and spatial density profiles of both particle populations (n_M for the Maxwellian group, and n_B for the beam) are constant within the well. It is of interest to calculate these Maxwellian and beam populations' densities, as well as the temperature of the confined Maxwellian population T , in terms of the input variables in the system, namely, S_{\max} and τ_i . The Maxwellian population loses particles at the top of the well at a rate given by¹⁹

$$\frac{\partial}{\partial t} (n_M)_{\text{loss}} \sim \frac{n_M}{\tau_M} \frac{T}{E_0} e^{-E_0/T},$$

where $\tau_M^{-1} = \sqrt{2} \pi e^4 \Lambda n_M / \sqrt{m} T^{3/2}$. Energy losses by upscattering at the top of the well are given in the same reference by

$$\frac{3}{2} \frac{\partial}{\partial t} (T n_M)_{\text{loss}} \sim \frac{n_M T}{\tau_M} e^{-E_0/T} \left[1 + \frac{3}{2} \frac{T}{E_0} \right].$$

Particles enter the well by downscattering from the beam, which here is represented by the beam downscattering rate $(\dot{n}_B)_d$. In equilibrium, particles introduced by the beam source (\dot{S}_B) can either downscatter and be confined in the well [at a rate given by $(\dot{n}_B)_d$], or they eventually get lost through the injection port at a rate given by n_B/τ_i . Hence, in collisional equilibrium, the beam particle balance equation reads

$$\dot{S}_B = (\dot{n}_B)_d + \frac{n_B}{\tau_i}.$$

The beam heats the confined Maxwellian at a rate given by $\nu_{\epsilon}^{B/M} n_B E_s$, where $\nu_{\epsilon}^{B/M}$ is the energy exchange frequency between a fast beam and a Maxwellian population of the same species, given by¹⁶

$$\nu_{\epsilon}^{B/M} \approx \frac{\mu}{\tau_M} \frac{T}{E_s} \left[\sqrt{\frac{T}{E_s}} - 1.1 \mu e^{-\mu(E_s/T)} \right],$$

where μ is the ion mass in proton mass units. Hence, the particle and energy balance equilibrium equations of the Maxwellian population read

$$\dot{S}_B - \frac{n_B}{\tau_i} = \frac{n_M}{\tau_M} \frac{T}{E_0} e^{-E_0/T}, \quad (16)$$

$$\nu_{\epsilon}^{B/M} n_B = \frac{n_M}{\tau_M} \frac{T}{E_s} e^{-E_0/T} \left[1 + \frac{3}{2} \frac{T}{E_0} \right]. \quad (17)$$

Energy transport of downscattered beam particles is considered small compared to beam heating, and has been neglected in Eq. (17). This set of two equations contains three unknowns, n_B , n_M , and T . Closure is provided by imposing that the total density be equal to the ion average density, $n_B + n_M = \langle n_i \rangle$.

These equations can be simplified further by using the following dimensionless variables: $\theta_b = \tau_i/\tau_{ii}$, $\hat{S}_B = \dot{S}_B(\tau_{ii}/\langle n_i \rangle)$, $\hat{n}_B = n_B/\langle n_i \rangle$, $\hat{n}_M = n_M/\langle n_i \rangle$, $\chi = \hat{n}_M/\hat{n}_B$, $\hat{T} = T/E_0$, $\hat{E}_s = E_s/E_0$, and read

$$\chi^2 \frac{e^{-1/\hat{T}}}{\sqrt{\hat{T}}} = (1 + \chi) \left[(1 + \chi) \hat{S}_B - \frac{1}{\theta_b} \right], \quad (18)$$

$$\chi = \mu e^{1/\hat{T}} \frac{\sqrt{\hat{T}/\hat{E}_s} - 1.1 \mu e^{-\mu \hat{E}_s/\hat{T}}}{1 + \frac{3}{2} \hat{T}}. \quad (19)$$

In this set of equations, the input variables are \hat{S}_B , \hat{E}_s (which characterize the source) and θ_b (which characterizes the sink), and the unknowns are χ (the ratio of Maxwellian to beam densities), and \hat{T} (the temperature of the Maxwellian population).

Equations (18) and (19) can be combined into a single nonlinear equation in terms of \hat{T} , which is solved numerically for each set of values $\{\hat{S}_B, \hat{E}_s, \theta_b\}$. Once \hat{T} is found, the energy gain of this simplified system can be calculated using Eq. (15). Care must be taken in calculating the volume-averaged reactivity $\langle \sigma v \rangle_{\text{vol}}$ with the semianalytic model, as nonuniform density profiles occur in the real system. Following Ref. 10, an effective reactivity $\langle \sigma v \rangle_{\text{eff}}$ can be defined as

$$\langle \sigma v \rangle_{\text{vol}} = \langle \sigma v \rangle_{\text{eff}} \int d(\hat{r}^3) \hat{n}_i^2(\hat{r}). \quad (20)$$

The density integral takes into account the effect of nonuniform density profiles on the reactivity. The actual value of the density integral is very much dependent on the density profile in the system, which varies widely according to the operating conditions. To have a feeling of the order of magnitude of the value of this density factor, the integral is calculated using a Gaussian density profile $\hat{n}_i(\hat{r}) = \hat{n}_0 \times \exp(-\hat{r}^2/\sigma^2)$, which is consistent with a Maxwellian distribution in a harmonic well. The width of the Gaussian σ is determined in terms of \hat{n}_0 so that $\hat{n}_i(\hat{r})$ averages to unity. The resulting density factor $\int d(\hat{r}^3) \hat{n}_i^2(\hat{r})$ is a mildly increasing function of the maximum density \hat{n}_0 , as shown in Fig. 5. Note that the density factor tends to one as $\hat{n}_0 \rightarrow 1$ (flat density profile). A density factor of $\int d(\hat{r}^3) \hat{n}_i^2(\hat{r}) \approx 2$ is assumed in subsequent calculations.

The effective reactivity $\langle \sigma v \rangle_{\text{eff}}$ is calculated in the semianalytic model as

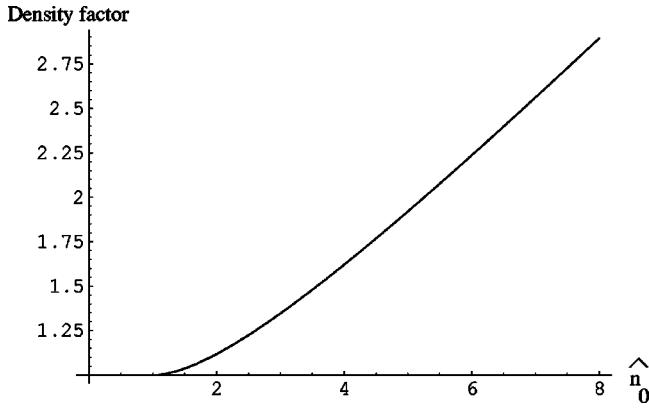


FIG. 5. Variation of the density factor in the reactivity with the maximum density \hat{n}_0 , assuming a Gaussian ion density profile $\hat{n}_i(\hat{r}) = \hat{n}_0 \times \exp(-\hat{r}^2/\sigma^2)$.

$$\begin{aligned} \langle \sigma v \rangle_{\text{eff}} &\approx \frac{n_B^2 \langle \sigma v \rangle_B(E_s) + n_M^2 \langle \sigma v \rangle_M(T)}{\langle n_i \rangle^2} \\ &= \frac{\langle \sigma v \rangle_B(E_0 \hat{E}_s) + \chi^2 \langle \sigma v \rangle_M(E_0 \hat{T})}{1 + \chi^2}. \end{aligned}$$

Here, we neglect the beam-Maxwellian contribution ($n_B n_M \langle \sigma v \rangle_{BM}$) for simplicity, and because we are interested in the limit where either the beam dominates or the Maxwellian dominates (see Sec. VI). The Maxwellian reactivity $\langle \sigma v \rangle_M$ is calculated using the fit proposed in Ref. 18; the reactivity for a monoenergetic beam in a spherical square well has been calculated in Ref. 10, and is employed here to estimate $\langle \sigma v \rangle_B$.

The normalized input power \hat{P}_{in} in Eq. (15) is approximated in the semianalytic model by

$$\hat{P}_{\text{in}} \approx \frac{4\pi}{3} \hat{S}_B (\hat{E}_s - 1), \quad (21)$$

where the constant is a geometric factor that takes into account the spherical volume integral in the real system.

In order to relate the results of the semianalytic model to the bounce-averaged Fokker-Planck model, it is necessary to express \hat{S}_B in terms of \hat{S}_{max} (which is the actual input parameter in the BAFP code). Although there is no rigorous rule available, a *heuristic* relation can be obtained by identifying the *normalized* particle input rate in BAFP with the particle source in the semianalytic model \hat{S}_B , as follows:

$$8\pi^2 \int d\hat{E} d\hat{L} \hat{S}(\hat{E}', \hat{L}) \approx 0.055 \hat{S}_{\text{max}} \sim \hat{S}_B,$$

where the integral has been calculated with $\hat{\sigma}_s = 0.035$. The best agreement between BAFP and the semianalytic model is in fact obtained with $\hat{S}_B \approx 0.04 \hat{S}_{\text{max}}$.

In this model, $Q \rightarrow \infty$ as $\hat{S}_{\text{max}} \rightarrow 0$. This limit is actually meaningless, because no real steady state occurs, and is an artifact of only including ion sources/sinks in the energy gain definition (which tend to zero as $\hat{S}_{\text{max}} \rightarrow 0$) and neglecting other sinks such as electron losses. The effects of electron

losses in the Q -value are briefly discussed in Sec. VIC (where it is shown that electron losses force $Q \rightarrow 0$ as $\hat{S}_{\text{max}} \rightarrow 0$).

VI. ENERGY GAIN RESULTS

In this section, a parametric study of the energy gain in Penning IEC devices operating with D-T fuel in *steady state* is performed to identify the region in the parameter space that offers the most efficient operating regimes. The space of *independent* input parameters of the bounce-averaged model is $\{\hat{E}_{\text{max}}, \hat{E}_{\text{dom}}, \hat{S}_{\text{max}}, \hat{E}_s, \hat{\sigma}_s, \gamma = n_e / \langle n_i \rangle, \theta = \tau_i / \tau_{ii}\}$, where a “^” indicates a dimensionless variable. Here, energies are normalized to the well depth E_0 , velocities are normalized to $v_0 = \sqrt{E_0/m}$, densities are normalized to the average ion density $\langle n_i \rangle$, times are normalized to τ_{ii} , and lengths are normalized to the cell radius a . The parametric study will focus on the following variables:

- (1) $\hat{S}_{\text{max}}, \hat{E}_s$, which characterize the ion source;
- (2) $\theta = \tau_i / \tau_{ii}$, which characterizes the ion sink;
- (3) $\gamma = n_e / \langle n_i \rangle$, which characterizes the well shape, and is directly related to the fusion power density in the system (via $\langle n_i \rangle$).

The rest of the input parameters will remain fixed in all simulations, to the following values: $\hat{E}_{\text{max}} = 1.2$, $\hat{E}_{\text{dom}} = 2.0$, and $\hat{\sigma}_s = 0.035$.

Energy gains are calculated with the BAFP code,¹¹ which integrates the nonlinear set of equations presented in Sec. IV. In order to compare the numerical energy gain results against previous theoretical results¹⁰ and the semianalytic model developed in Sec. V, the system is analyzed first with a square potential well. Modifications of these results for more realistic potential wells are presented in Sec. VI B; in particular, perfectly parabolic wells (the case when ions do not appreciably affect the electron space charge) and quasi-parabolic wells (resulting from partial ion neutralization of the electron space charge) are discussed in detail. Power density issues and the effect of electron losses on the energy gain are discussed in Sec. VIC.

A. Square well

Three parameters are relevant in this scenario, namely, $\{\hat{S}_{\text{max}}, \hat{E}_s, \theta\}$. Recall that θ is the normalized ion replacement time, and hence, larger θ -values correspond to weaker sinks, and vice versa. The following values are considered for this study:

- (1) $\theta = \{0.1, 0.01, 0.001\}$, consistently with the time ordering in Sec. III B;
- (2) $\hat{S}_{\text{max}} = \{30, 300\}$, to provide different beam-Maxwellian equilibria [typically, $\hat{S}_{\text{max}} = 300$ results in focused, beam-like steady-state solutions, while $\hat{S}_{\text{max}} = 30$ results in a truncated Maxwellian distribution (which “fills” the well) with a small beam-like contribution¹¹];
- (3) $\hat{E}_s = \{1.04, 1.09, 1.14\}$. These values are in between the

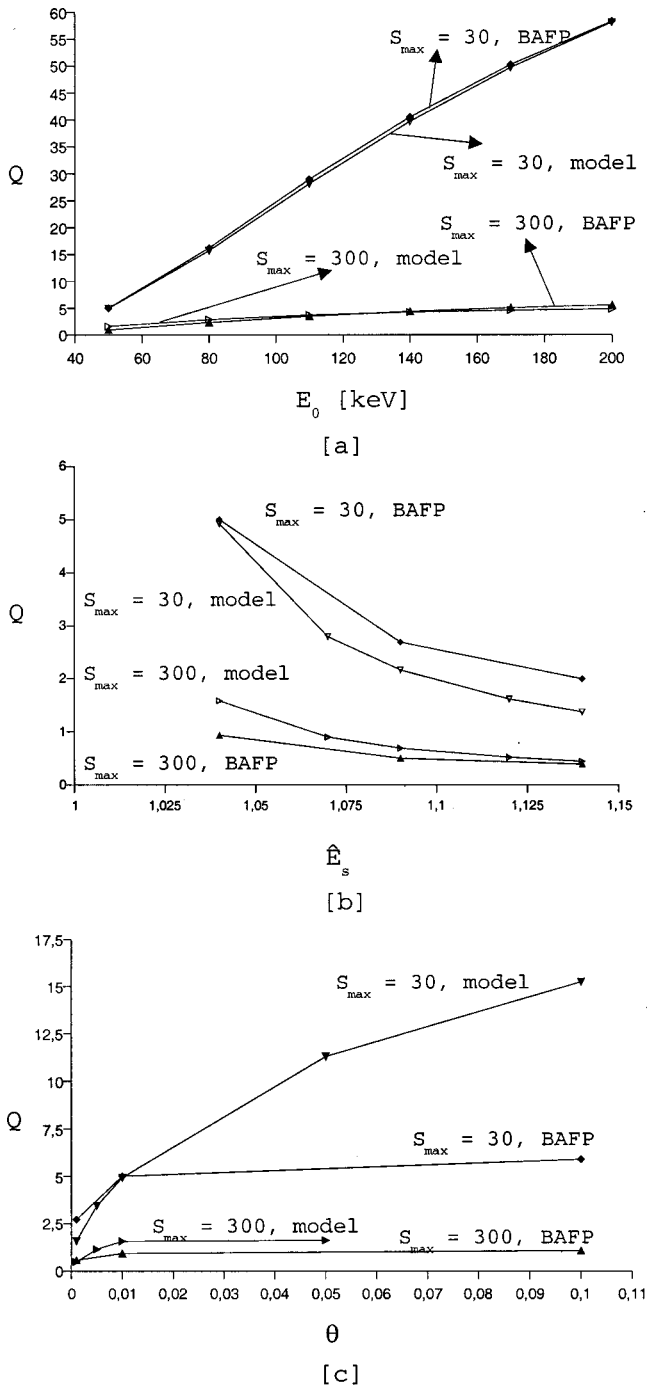


FIG. 6. Scaling of the energy gain calculated with BAFP for a square potential well with (a) the well depth E_0 , (b) the beam injection energy \hat{E}_s (specialized for $\theta=0.01$ and $E_0=50$ keV), and (c) the normalized ion replacement time θ (specialized for $\hat{E}_s=1.04$, $E_0=50$ keV). Results for the same parameters obtained with the semianalytic model are also included for comparison.

well depth ($\hat{E}_0=1$) and the potential at the wall ($\hat{E}_{\max}=1.2$), and correspond to ion injection energies 4%–14% above the well depth.

Results of the energy gain calculations with BAFP are presented in Fig. 6. Figure 6(a) depicts the scaling of the Q -value with the well depth E_0 (in keV), for the two values

of \hat{S}_{\max} under consideration, and detailing the results for $\theta=0.01$ and $\hat{E}_s=1.04$. Results from the semianalytic model are also included for reference (with $\theta_b \approx \theta$ and $\hat{S}_B \approx 0.04\hat{S}_{\max}$). Note that the semianalytic model reproduces both the trends and magnitude of the results obtained with BAFP. From these plots, we see that weak ion sources (which correspond to Maxwellian-dominated solutions) result in a stronger scaling of Q with the well depth, and that well depths >100 keV are required for large Q . This counterintuitive result can be readily understood by recalling that the Maxwellian component of the solution is almost absolutely confined by the electrostatic well, whereas the beam component is only partially confined (Sec. IV A). Thus, a small beam component results in less recirculating power—and hence larger Q -values—for the same average particle energy.

The scaling of Q with \hat{E}_s obtained with BAFP for $E_0=50$ keV is shown in Fig. 6(b); clearly, Q improves as \hat{E}_s decreases. Results from the semianalytic model largely agree with BAFP's; however, their scalings differ slightly as $\hat{E}_s \rightarrow 1$. This is an artifact of the approximation used for the input power in the semianalytic model [Eq. (21)], since $\hat{P}_{\text{in}} \rightarrow 0$ as $\hat{E}_s \rightarrow 1$ (and hence $Q \rightarrow \infty$), while the input power in BAFP remains finite as $\hat{E}_s \rightarrow 1$ [due to the ion source spread in (E, L) space].

The variation of Q with θ obtained with BAFP is plotted in Fig. 6(c), indicating that Q is quite insensitive to variations in the sink strength for $\theta > 0.01$, and it decreases rapidly for θ below that threshold. This behavior is consistent with a power law of the type $Q \sim \theta^\alpha$, where $\alpha \ll 1$ (theoretical estimates^{10,12} of α for monoenergetic beams yield $\alpha = 1/4$), and indicates that it is crucial for large Q to design fusion cells with mild ion sinks ($\theta > 0.01$ implies, according to Sec. III B, $f_D < 10^{-5}$; this requirement is relaxed for realistic potential profiles and very large well depths, as indicated in Sec. VI B). Although the semianalytic model and BAFP agree in order of magnitude and trend in the beam-dominated solution ($\hat{S}_{\max}=300$), for the Maxwellian-dominated solution ($\hat{S}_{\max}=30$) the semianalytic trend grows faster than BAFP's (i.e., the exponent α is larger for the semianalytic model). This occurs because (1) Maxwellian solutions are more sensitive to changes in the sink strength than beam-like solutions, due to the nonlinear dependence of \hat{T} on the sink parameter, and (2) for the same variation of θ (BAFP) and θ_b (semianalytic model), changes in the sink strength in the semianalytic model are more drastic than changes in the sink strength in BAFP, particularly near the top of the well E_0 [because the semianalytic model assumes a constant sink strength $1/\theta_b$ in the slow ion loss region ($E_0 < E' < E_{\max}$), while the sink strength in BAFP follows a linear profile that increases from zero at $E'=E_0$ up to $1/\theta$ [Eq. (6)].

1. Comparison with previous theoretical work

Energy gains for spherical IEC systems have been estimated theoretically in Ref. 10, where a monoenergetic ion distribution function (modeled with a Dirac delta) confined

TABLE I. Comparison of analytical and numerical estimates of Q -values in a beam-dominated solution for a 50 kV square well.

	Analytical	BAFP
With co-moving ions	$Q < 0.21$ (Ref. 10)	...
Without co-moving ions	$Q < 1.3$ (Ref. 12)	$Q \sim 1$

in a square potential well was employed to calculate collisional relaxation rates and estimate the ion pumping power required to sustain such a distribution in steady state. The calculation suggested that

- (1) Gains are limited to $Q < 0.21$ for a 50 kV well depth.
- (2) Q increases mildly with the well depth E_0 .
- (3) $Q \sim \sqrt{\rho_0}$, where $\rho_0 = r_0/a$, and r_0 is the radius of a constant-density central core. In the same reference, $\theta \sim \rho_0^2$, and hence $Q \sim \theta^{1/4}$. Thus, Q increases mildly with θ .

These conclusions cannot be compared directly with the results from the bounce-averaged Fokker–Planck model because of the impossibility of implementing delta functions numerically. However, BAFP should reproduce the same phenomenology in the case of beam-like steady-state ion distribution functions. This is in fact the case, because

- (1) Q increases mildly with E_0 in the beam-like solution limit [$\hat{S}_{\max} = 300$ in Fig. 6(a)].
- (2) Q increases very mildly with θ [Fig. 6(c)].

However, calculated Q -values from BAFP in the *beam-like case* are about five to ten times larger than those obtained in Ref. 10 (see Table I). This inconsistency can be traced back to the different treatment of the D and T ion species in both calculations. Thus, while BAFP treats both species as one with average mass $m = (m_T + m_D)/2$, Ref. 10 treats both species separately but assuming they follow the *same* monoenergetic distribution function. This results in a finite velocity difference between species that boosts collisionality, rendering smaller Q -values. The inconsistency in the Q -value disappears when BAFP is compared against theoretical estimates with a similar multispecies treatment,¹² as shown in Table I.

Results so far have been obtained for a very simplified well shape (the square well). Realistic wells with a quasiuniform electron cloud are parabolic-like, with corrections due to the ion self space charge. Energy gain results for these more realistic wells are given next.

B. Self-consistent wells

The term “self-consistent” refers here to the fact that the potential profile is consistent with Poisson’s equation, with the assumption that electrons retain a uniform density profile. The well shape in this situation is determined by the ratio of the electron to ion average volumetric densities, $\gamma = n_e / \langle n_i \rangle$. In order to provide adequate ion confinement, electrons have to be in excess; hence, $\gamma > 1$. Here, two limits are considered:

- (1) $\gamma \gg 1$ (parabolic): the perturbation of the ion self space charge on the potential well profile is negligible, and the well remains parabolic. Thus, it is not required to solve the nonlinear Poisson problem. This limit provides the deepest wells (thus increasing the fusion reactivity), but fusion power densities are low because of small average ion densities (the electron density is considered fixed, because it is determined by technological and design considerations).
- (2) $\gamma > 1$ (quasiparabolic): electrons are in excess, but the ion perturbation on the potential well profile cannot be neglected, and the potential profile has to be recalculated every time step. The partial neutralization of the electron space charge reduces the well depth available for ions, thus decreasing the fusion reactivity. However, the fusion power density increases because, according to the definitions of P_f , $\langle \sigma v \rangle_{\text{vol}}$, and γ , $P_f \propto \langle \sigma v \rangle_{\text{vol}} n_e^2 / \gamma^2$, showing that small γ -values are preferable. Here, $\gamma = 5$ is selected (which typically reduces the available well depth by a half).

To provide a fair comparison of the energy gains in both limits, the effective well depth—after partial neutralization—is used in the plots. The comparison has been done for $\hat{E}_s = 1.04$ only, because the evolution of the Q -value with \hat{E}_s is well-known [$Q \sim 1/(\hat{E}_s - 1)$], and this case results in best energy gains.

The Q -value phenomenology in self-consistent wells will vary from that observed in the square well case, for the following reasons:

- (1) While in square wells the beam component is solely responsible for any density peaking at $r=0$ (see Fig. 8 below) due to ion focusing, in parabolic-like wells the thermal component may also contribute to density peaking. This occurs because the density profile of the Maxwellian component follows the Boltzmann factor, $e^{-e\Phi(r)/k_B T} \approx e^{-\hat{r}^2/\hat{T}}$, which peaks at $r=0$. Hence, for the same ion distribution, the density profile will generally be sharper in parabolic wells than in square wells due to the thermal component contribution, and will result in larger density peaks to satisfy the integral condition $\int_0^1 d(\hat{r}^3) \hat{n}(\hat{r}) = 1$.
- (2) The parabolic profile results in less average ion kinetic energy per bounce, because some is transformed back into potential energy in each ion oscillation in the trap.

These two effects influence the fusion power in opposite ways. On the one hand, more peaked density profiles increase the fusion power (via the density factor). On the other hand, in the case of the average kinetic energy being below the Maxwellian D-T fusion reactivity peak (located at $T \approx 60$ keV), smaller average ion kinetic energies decrease the fusion power (via the fusion reactivity).

The density peaking and the average kinetic energy also affect the ion input power via the ion-ion collision frequency. In general, *for a fixed source strength*, increasing the density peaking and/or decreasing the average ion kinetic energy per ion bounce results in larger ion-ion collision fre-

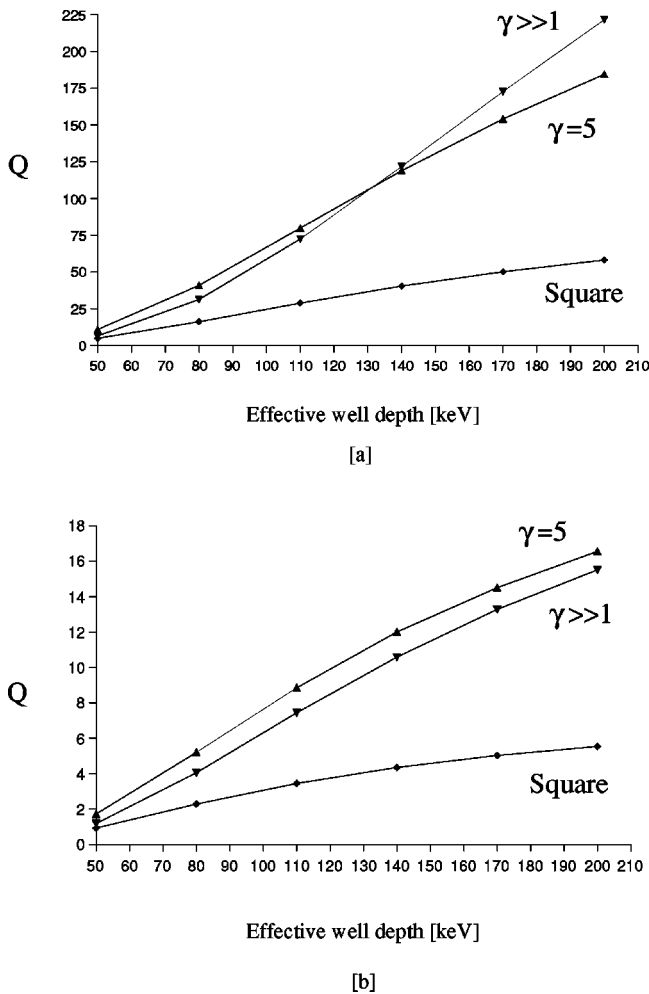


FIG. 7. Comparison of the scaling of the energy gain Q with the effective well depth for different well shapes ($\gamma=5, \gg 1$, and square well) for (a) $\hat{S}_{\max}=30$, and (b) $\hat{S}_{\max}=300$. These plots have been obtained with $\hat{E}_s = 1.04$ and $\theta=0.01$.

quencies, and hence in larger input power requirements. However, the input power will only be affected significantly when the Maxwellian component is dominant, because it is then that power losses due to ion-ion collisions are relevant (via the Pastukhov factor¹⁹).

The overall influence of these different effects on the Q -value is not obvious *a priori*, because it depends on the relative change of the fusion power and the ion input power. Figure 7 depicts the scaling of the Q -value with the effective well depth for both weak sources [$\hat{S}_{\max}=30$, Fig. 7(a)] and strong sources [$\hat{S}_{\max}=300$, Fig. 7(b)]. Scalings for parabolic and quasiparabolic wells are shown, together with those for the square well (which are included for comparison). In this figure, the Q -values in shallow wells ($E_0 \sim 50$ keV) are similar for all well shapes, indicating that, in parabolic-like wells, the input power and kinetic energy effects offset the density peaking effect. However, as the well depth is increased, the kinetic energy effect becomes unimportant and the density peaking effect dominates over the input power effect, resulting in Q increasing faster with E_0 in parabolic-like wells than in square wells. Note in Fig. 7 that weak ion sources

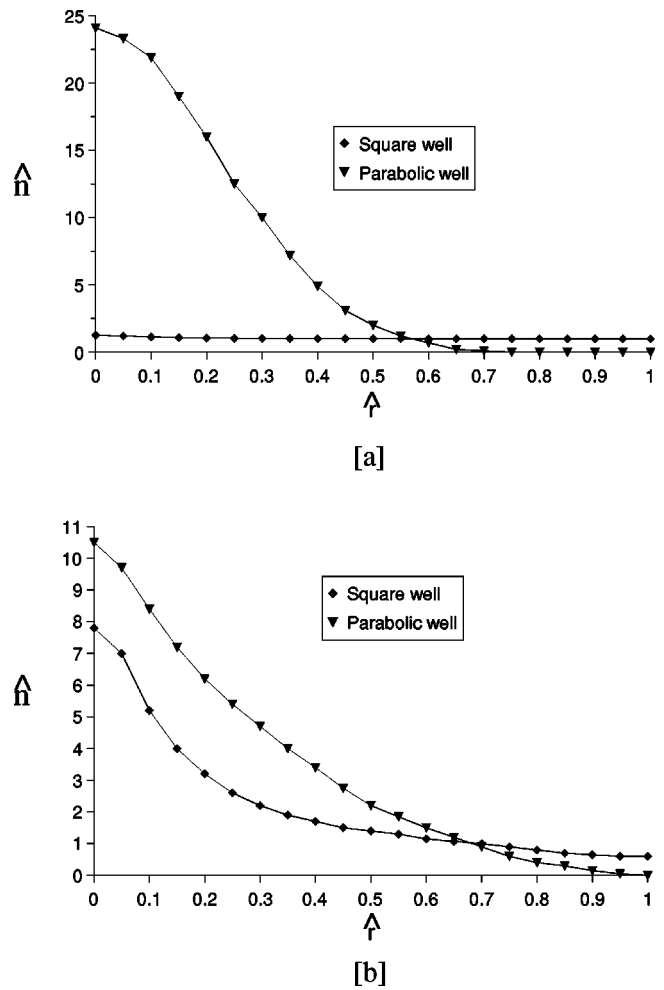


FIG. 8. Plot of the density profiles $\hat{n}(\hat{r})$ in square and parabolic wells resulting from (a) a quasithermal solution ($\hat{S}_{\max}=30$ and $\theta=0.001$), and (b) a beam-like solution ($\hat{S}_{\max}=300$ and $\theta=0.1$).

also result in better Q -values than strong sources for parabolic-like wells, due to the smaller recirculation powers required to maintain the steady-state solution.

Figure 8 shows the density profiles obtained with BAFP in both the quasithermal [Fig. 8(a)] and beam-like [Fig. 8(b)] limits. All density profiles in this figure satisfy the integral condition $\int_0^1 d(\hat{r}^3) \hat{n}(\hat{r}) = 1$, and hence the number of particles is the same in all cases (note that large density differences at small radii may be offset by small density differences at large radii because the density is weighed by a factor \hat{r}^2 in the normalization integral). The ratio of the density factor for the parabolic well to that for the square well is ~ 8 in the quasithermal case, and ~ 3 in the beam-like case, while the energy gain ratio at large well depths (Fig. 7) is ~ 5 in the quasithermal case, and ~ 3 in the beam-like case. The energy gain ratio in the quasithermal case is somewhat smaller than the corresponding density factor ratio due to the simultaneous increase in the input power. On the other hand, the beam-like energy gain ratio is of the order of the corresponding density factor ratio, consistently with the observation that the input power effect is only relevant in quasithermal solutions.

The competing density and kinetic energy effects have

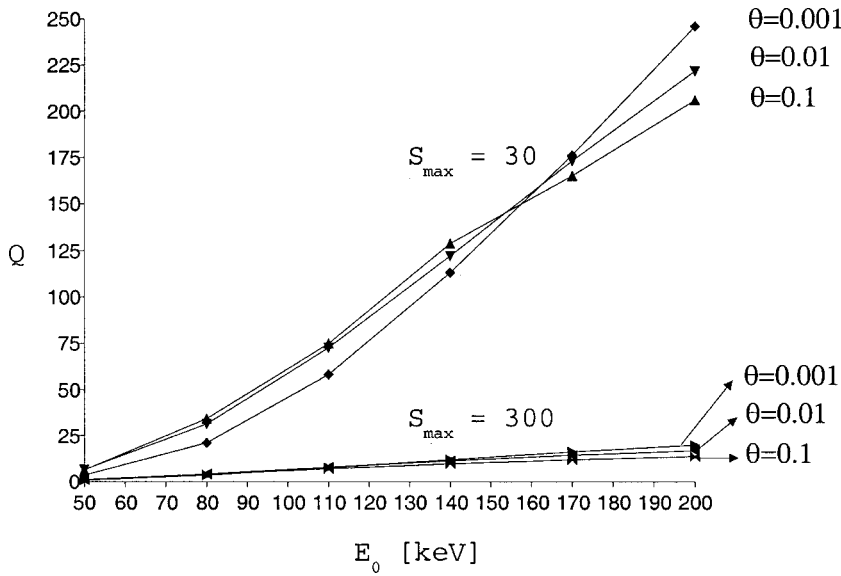


FIG. 9. Plot of the Q -value as a function of the well depth E_0 for the purely parabolic well case ($\gamma \gg 1$), for $\theta = 0.001, 0.01, 0.1$, and for $\hat{S}_{\max} = 30$ and $\hat{S}_{\max} = 300$.

interesting consequences in the scaling of the Q -value with the normalized ion replacement time, θ . This is shown in Fig. 9. Thus, while the Q -value increases slightly with θ for shallow electrostatic wells, the trend is reversed for large electrostatic wells ($E_0 > 150$ kV), for which the Q -value actually increases as θ decreases (i.e., as the sink grows stronger). This effect is more noticeable in quasithermal solutions ($\hat{S}_{\max} = 30$) than in beam-like solutions ($\hat{S}_{\max} = 300$) because in the former the density peak is strongly dependent on \hat{T} , which in turn is nonlinearly dependent on θ . Thus, larger sinks (smaller θ) result in smaller normalized temperatures—to limit the Maxwellian tail losses—which in turn increases the Q -value in two ways: (1) it results in larger density peaks [consistently with the Boltzmann factor $\hat{n}(\hat{r}) \propto e^{-\Phi \hat{T}}$ and the normalization condition], and (2) for extremely large well depths ($E_0 > 150$ – 200 kV), the absolute ion temperature may rise above the Maxwellian D-T fusion reactivity peak (which is located at $T \approx 60$ keV), and hence smaller temperatures may result in larger fusion reactivities.

From these results, it is clear that self-consistent wells have better convergence and energy multiplication properties than square wells, and the corresponding Q -values are less sensitive to the sink strength, provided that operation at large well depths ($E_0 > 150$ kV after neutralization) is possible experimentally.

However, a direct quote of these energy gain results may be misleading, because the calculation of the Q -value in this model includes only ion losses, and neglects electron losses in the system. The effects of these losses on the Q -value are heuristically discussed in the next section.

C. Heuristic estimate of the effect of electron losses in the energy gain

Preliminary conclusions on the influence of electron power losses in the energy gain of the system can be drawn using the semianalytic model developed in Sec. V (which applies only to square wells). Electron energy may be lost by

electron upscattering from the electron well, $P_{e,\text{loss}}$, and radiative losses due to the presence of ions in the system, P_{Br} (it is assumed that no electrons are lost to the anode or the ion extraction grid). Electron upscattering losses are estimated by

$$P_{e,\text{loss}} \sim f_e \frac{4\pi a^3}{3} \frac{n_e \Delta E_{\perp}}{\tau_{ee}}, \quad (22)$$

where ΔE_{\perp} is the perpendicular energy carried out by electrons [which is gyrating energy due to the presence of the axial magnetic field and is assumed to be of the order of the electron injection energy in the system (\sim eV)], $\tau_{ee} = \sqrt{m_e} W_0^{3/2} / \sqrt{2} \pi (k_0 e^2)^2 n_e \Lambda_e$ is the electron collision time (where $W_0 \sim 3E_0$ is the electron well depth¹³), and f_e is a nonphysical factor that controls the electron upscattering losses, and will be used to address the sensitivity of the Q -value to this power loss mechanism.

Radiative losses are estimated using the well-known expression for Bremsstrahlung losses of a Maxwellian electron population,

$$P_{\text{Br}} \approx \frac{4\pi a^3}{3} A_{\text{Br}} \langle n_i \rangle n_e \sqrt{k_B T_e}, \quad (23)$$

where T_e is the electron temperature, k_B is the Boltzmann constant, and $A_{\text{Br}} = 1.6 \cdot 10^{-38} \text{ m}^3 \text{ J} / \sqrt{e} \text{ V s} = 4 \cdot 10^{-29} \text{ m}^3 \sqrt{\text{J/s}}$. In this application, electrons are close to monoenergetic with energy W_0 . Thus, $(3/2)k_B T_e \sim W_0$ is assumed.

The dimensionless forms of Eqs. (22) and (23) read

$$\hat{P}_{e,\text{loss}} = \frac{4\pi}{3} \sqrt{\frac{m_i}{m_e}} \left(\frac{E_0}{W_0} \right)^{3/2} \Delta \hat{E}_{\perp} f_e \gamma^2 = \frac{4\pi}{3} Q_e f_e \gamma^2,$$

$$\hat{P}_{\text{Br}} = \frac{4\pi}{3} A_{\text{Br}} \frac{\sqrt{m_i}}{\sqrt{2} \pi (k_0 e^2)^2 \Lambda} \sqrt{\frac{2W_0}{3E_0}} \gamma E_0 = \frac{4\pi}{3} Q_{\text{Br}} \gamma E_0.$$

For a 100 kV well and $W_0 \sim 3E_0$, we find $Q_e \approx 1.3 \cdot 10^{-3}$ and $Q_{\text{Br}} \approx 1.2 \cdot 10^{-4} \text{ keV}^{-1}$. Then, the energy gain reads

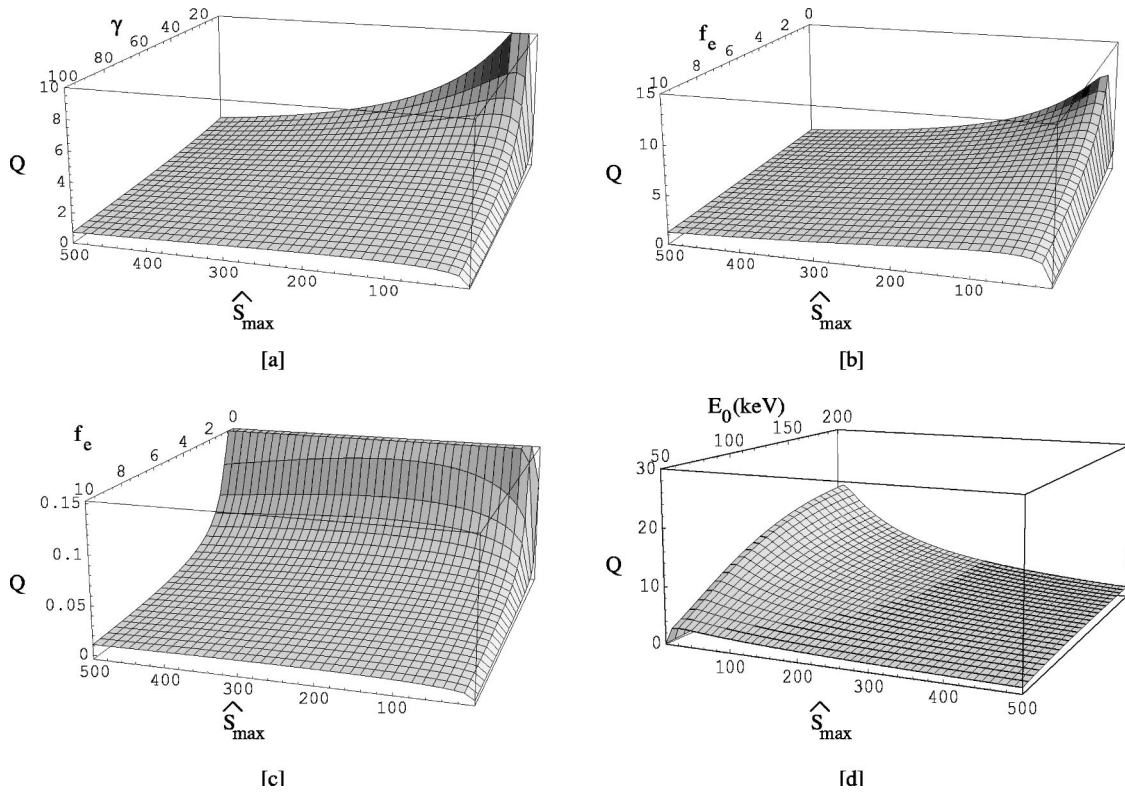


FIG. 10. Plot of the Q -value (including electron losses) as a function of (a) \hat{S}_{\max} and γ with $f_e=10^{-3}$, (b) \hat{S}_{\max} and f_e with $\gamma=5$, (c) \hat{S}_{\max} and f_e with $\gamma=100$, and (d) \hat{S}_{\max} and E_0 with $\gamma=5$ and $f_e=10^{-3}$. These plots have been obtained for $E_0=100$ keV [except (d)], $\theta_b=0.01$, and $\hat{E}_s=1.04$.

$$Q \approx \frac{Y_{\text{fuel}} K_{\text{fuel}} \sqrt{m E_0} \langle \sigma v \rangle_{\text{vol}}}{\sqrt{2} \pi (k_0 e^2)^2 \Lambda [0.04 \hat{S}_{\max} (\hat{E}_s - 1) + Q_e f_e \gamma^2 + Q_{\text{Br}} \gamma E_0]}, \quad (24)$$

with $\langle \sigma v \rangle_{\text{vol}}$ determined from Eq. (20). This expression of the Q -value explicitly includes the electron to ion density ratio γ , and the sensitivity factor f_e . Note that the energy gain is monotonically decreasing with both of these parameters. The dependence of the energy gain on γ for different source strengths \hat{S}_{\max} is shown in Fig. 10(a) for $E_0=100$ keV, $\theta_b=0.01$, $\hat{E}_s=1.04$, and $f_e=10^{-3}$. Clearly, smaller values of γ result in best energy gains (although γ has to be sufficiently large to maintain the negative space charge), consistently with power density arguments (recall $P_f \sim 1/\gamma^2$). Note that $Q \rightarrow 0$ as $\hat{S}_{\max} \rightarrow 0$ (instead of growing to infinity). There is in fact an optimal source strength that, while allowing a quasithermal ion distribution, provides sufficient power density to overcome the electron losses.

The effect of f_e on the Q -value is depicted in Figs. 10(b), 10(c), for several scenarios of γ ($\gamma=5, 100$). Figure 10(b) shows the dependence of Q on f_e and \hat{S}_{\max} , for $\gamma=5$. While the Q -value is insensitive to f_e for large source strengths, it is quite sensitive for small source strengths (the case of interest here). Note that very large Q -values can be achieved for $\gamma=5$ if $f_e \rightarrow 0$, which implies achieving excellent electron particle confinement (so the only remaining electron loss is Bremsstrahlung).

For $\gamma=100$, however, the situation is quite different [Fig. 10(c)]. The sensitivity of Q to f_e increases signifi-

cantly, as might be expected, since f_e in Eq. (24) is multiplied by γ^2 . However, in this regime, $Q < 1$ even when $f_e = 0$, because the fusion power density is too low to overcome Bremsstrahlung losses.

Finally, the scaling of the Q -value with the well depth and the source strength for $\gamma=5$ and $f_e=10^{-3}$ is depicted in Fig. 10(d). The scaling is best for the optimal source strength. Achieving large Q -values requires well depths > 100 keV.

VII. CONCLUSIONS

In this paper, a bounce-averaged Fokker-Planck model has been employed to obtain steady-state solutions for the ion distribution function—and to calculate associated fusion energy gains (Q -values)—in a variety of operating conditions in terms of source and sink strengths, ion injection energies, well depths and electrostatic potential shapes.

Prior analyses of the Q -value of IEC devices¹⁰ have assumed that ions were confined in a *square* potential well, and that their distribution was tightly focused and monoenergetic. With these premises, estimated Q -values were typically less than 0.2. However, when these restrictive assumptions are relaxed, it is found that large energy gains ($Q \sim 10$) for *beam-like* solutions in square wells are possible in Penning IEC devices provided that

- (1) The electrostatic well is deep enough ($E_0 > 100$ keV);
- (2) Ion confinement time is long enough ($\theta > 0.01$);
- (3) Ion source strength is moderate ($\hat{S}_{\max} < 300$);

- (4) Ion injection energy is close to the top of the well ($E_s \approx 1.04 - 1.14E_0$).

In addition, novel, very efficient ($Q \sim 50$) operating regimes have been identified in deep square wells for weak ion sources ($\hat{S}_{\max} \sim 30$) and moderately long ion confinement times ($\theta \sim 0.01$), in which the Maxwellian contribution is dominant over the beam contribution. These results indicate that efficient use of the electrostatic well is essential to achieve large fusion gains, and demonstrate that the Maxwellian ion distribution—which has been neglected in previous analyses—might also be of interest for the inertial electrostatic confinement concept.

Results also indicate that the square well assumption, used in previous analytical estimates,^{3,10} is in fact a pessimistic one. Thus, *parabolic* wells result in larger density peaks at the center, yielding Q -values 3 to 5 times larger (for $E_0 > 150$ kV) than those obtained with square wells, and are more forgiving with respect to the sink strength.

Preliminary studies of the effects of electron particle and radiative losses indicate that large Q -values are still possible if Penning IEC devices operate with small electron to ion density ratios, at the optimal ion source strength (small enough to allow a quasithermal solution, but large enough to provide sufficient fusion power density in the system to overcome electron power losses), provided that electron particle losses are small ($0 < f_e < 1$) and well depths are large ($E_0 > 100$ kV).

ACKNOWLEDGMENTS

The authors wish to acknowledge useful conversations with Dr. John Finn from Los Alamos National Laboratory.

This research has been partially supported by the U.S. Department of Energy, and by the NCSA under Grant No.

PHY990011N (this work utilized the NCSA SGI/CRAY Origin 2000). L.C. has been funded by a Fellowship of the Spanish Ministry of Education and Culture, and this research is part of his Ph.D. dissertation at the University of Illinois.

¹R. W. Bussard, *Fusion Technol.* **19**, 273 (1991).

²N. A. Krall, *Fusion Technol.* **22**, 42 (1992).

³T. H. Rider, *Phys. Plasmas* **2**, 1853 (1995).

⁴D. C. Barnes, T. B. Mitchell, and M. M. Schauer, *Phys. Plasmas* **4**, 1745 (1997).

⁵D. C. Barnes, *Phys. Plasmas* **6**, 4472 (1999).

⁶T. B. Mitchell, M. M. Schauer, and D. C. Barnes, *Phys. Rev. Lett.* **78**, 58 (1997).

⁷M. M. Schauer, T. B. Mitchell, M. H. Holtzscheiter, and D. C. Barnes, *Rev. Sci. Instrum.* **68**, 3340 (1997).

⁸D. C. Barnes, M. M. Schauer, K. R. Umstadter *et al.*, *Phys. Plasmas* **7**, 1693 (2000).

⁹K. R. Umstadter, M. M. Schauer, and D. C. Barnes, *Phys. Rev. Lett.* (submitted).

¹⁰W. M. Nevins, *Phys. Plasmas* **2**, 3804 (1995).

¹¹L. Chacón, D. C. Barnes, D. A. Knoll, and G. H. Miley, *Comput. Phys. Commun.* (in press).

¹²T. N. Tiourine and D. C. Barnes, *Bull. Am. Phys. Soc.* **40**, 1665 (1995).

¹³M. M. Schauer, PFX-I (Penning Fusion eXperiment-Ions), 1997, proposal submitted to the Office of Fusion Energy, Office of Energy Research, U.S. Department of Energy, in response to the Program Announcement LAB97-08 "Innovations in Fusion Energy Confinement Systems." See EPAPS Document No. E-PHPAEN-7-935005 for PFX-I proposal. This document may be retrieved via the EPAPS homepage (<http://www.aip.org/pubservs/epaps.html>) or from <ftp.aip.org> in the directory /epaps/. See the EPAPS homepage for more information.

¹⁴R. Nebel and D. C. Barnes, *Fusion Technol.* **34**, 28 (1998).

¹⁵D. C. Barnes and R. A. Nebel, *Phys. Plasmas* **5**, 2498 (1998).

¹⁶J. D. Huba, *NRL Plasma Formulary*, *NRL/PU/6790-98-358* (Naval Research Laboratory, Washington, DC, 1998).

¹⁷M. N. Rosenbluth, W. M. Macdonald, and D. L. Judd, *Phys. Rev.* **107**, 1 (1957).

¹⁸H. S. Bosch and G. M. Hale, *Nucl. Fusion* **32**, 611 (1992).

¹⁹V. P. Pastukhov, *Nucl. Fusion* **14**, 3 (1974).